Early signaling pathways during *in vitro* culture of isolated primordial follicles

Running Title: Primordial follicle programmed cell death

Pritha Dey[1], Noemi Monferini[1], Ludovica Donadini[1], Filippo Zambelli[2], Maria Belen Rabaglino[3], Valentina Lodde[1], Federica Franciosi[1] and Alberto Maria Luciano[1,*]

[1]Reproductive and Developmental Biology Laboratory (ReDBioLab), Department of Veterinary Medicine and Animal Sciences, University of Milan, Milan, Italy; [2]Eugin Group, Barcelona, Spain; [3]Department of Population Health Sciences, Faculty of Veterinary Medicine, Utrecht University, Netherlands.

[*]**Correspondence Address:** Alberto Maria Luciano, Reproductive and Developmental Biology Laboratory (ReDBioLab), Department of Veterinary Medicine and Animal Sciences, University of Milan, Via dell'Università, 6 - 26900 Lodi, Italy – Phone (+39) 02 50334348 – e-mail: alberto.luciano@unimi.it ; ORCID: https://orcid.org/0000-0002-8016-9919

PD: https://orcid.org/0000-0002-1601-6379

NM: https://orcid.org/0000-0002-2339-9953

LD: https://orcid.org/0009-0005-9258-9047

FZ: https://orcid.org/0000-0001-7275-2947

MBR: https://orcid.org/0000-0002-0099-045X

VL: https://orcid.org/0000-0002-9768-2292

FF: https://orcid.org/0000-0001-8742-0291

© The Author(s) 2025. Published by Oxford University Press on behalf of the European Society of Human Reproduction and Embryology. All rights reserved. For permissions, please e-mail: journals.permission@oup.com

Abstract

The ability to grow undifferentiated oocytes *in vitro* from primordial follicles would increase the availability of fully grown oocytes in fertility preservation programs and other downstream applications. To date, the development of living offspring *in vitro* from the primordial follicle reserve has only been achieved in mice, proving the principle of the potential value of follicle culture as a source of competent oocytes. In certain pathophysiological conditions, such as polycystic ovarian syndrome, premature ovarian failure, or ovarian and blood cancer, where the ovarian tissue cannot be reintroduced into the patient, it is essential to isolate these follicles from the surrounding tissue and culture them *in vitro*. However, the culture systems that produce mature oocytes from isolated primordial follicles are still under investigation. Upon isolation from the ovarian microenvironment, a critical limiting factor is follicle death after a short period of culture. Previous studies suggest that glycine, a key component of glutathione (GSH), plays a protective role against the programmed cell death mechanism, ferroptosis, in *in vitro* matured porcine oocytes via the System X_c^- /GSH/glutathione peroxidase 4 (GPX4) axis. Employing a previously developed high-yielding primordial follicle mechanical isolation strategy and a defined culture system, we used RNA-seq to advance the knowledge of the main transcriptional events and molecular factors determining follicle fate in a 2D culture system. Our transcriptome analyses identified genes involved in ferroptosis that may bring about primordial follicle death. To suppress ferroptosis, glycine supplementation maintained the viability of primordial follicles at approximately 85% for 16 hours. Future improvements to the culture system should inhibit programmed cell death mechanisms and ensure the physiological compliance of the genes regulating primordial follicle activation and transition to the primary stage, along with effective

supplementation media to develop isolated primordial follicles *in vitro*.

Key Words

Bovine, Primordial Follicle, Folliculogenesis, Ovarian Reserve, Mechanical Isolation, *In vitro* Culture, RNA-seq, Programmed cell death, Ferroptosis, Glycine

Introduction

Current ART procedures primarily utilize advanced follicle stages for *in vitro* embryo production. In large mammals like the bovine, ARTs can rely only on the limited population of fully-grown oocytes isolated from medium to large antral follicles (Luciano *et al.*, 2021) and, with lower success, on growing oocytes isolated from early antral follicles (Garcia Barros *et al.*, 2023). Meanwhile, developing competent oocytes from the significant reserve of preantral follicles through isolation and culture remains an ongoing challenge (Telfer *et al.*, 2023).

The preantral follicles, in decreasing order of size, include secondary (SF), primary (PF), and primordial follicles (PMF). In women, the ovarian reservoir consists of 700,000 – 1,00,0000 PMF at birth (Gougeon *et al.*, 1994, Hansen *et al.*, 2008) and declines with age, leading to the progressive depletion of the ovarian reserve. In conditions like premature ovarian insufficiency, it is essential to isolate follicles from the surrounding environment and culture them *in vitro* for the subsequent stages of development. Similarly, ovarian grafts cryopreserved before radiotherapy or chemotherapy cannot always be transferred back to the patients for the risk of inducing recurrencies, as in the case of ovarian or blood cancers (Bastings *et al.*, 2013, Salama *et al.*, 2016). In mice, the potential of *in vitro* folliculogenesis has been soundly demonstrated through a two-step culture whereby ovaries, at first and individual follicles later, were cultured to generate mouse pups (O'Brien *et al.*, 2003). Conversely, in large mammals like humans and cattle, only limited success of the development of PMF to the secondary follicle stage *in situ,* i.e., within a fragment of tissue, was obtained with micro-cortex culture (Araujo *et al.*, 2014, Mclaughlin *et al.*, 2018, Simon *et al.*, 2020, Telfer *et al.*, 2019). However, the culture of tissue fragments is accompanied by the inherent inability to monitor follicle progression

during the culture period. For instance, the percentage of PMF reaching the PF stage versus those dying in the process cannot be accurately accounted for.

To overcome pathophysiological and technical issues, isolation procedures have been optimized to maximize the number of PMF recovered from a small volume of cortical tissue while retaining the maximum viability of freshly isolated follicles at time zero (T0) (Dey *et al.*, 2024a, Langbeen *et al.*, 2015, Monferini *et al.*, 2024).

Previous studies showed that *in vitro* development of preantral follicles can be influenced by follicle size, among other properties (Katska and Rynska, 1998, Saha *et al.*, 2000). Preantral follicles have distinct morphological features (Chen *et al.*, 2022, Fair *et al.*, 1997, Gougeon, 1986, Grosbois *et al.*, 2023, Monferini *et al.*, 2024, Wang *et al.*, 2020a, Zhang *et al.*, 2018). PMF are quiescent follicles with an oocyte surrounded by flattened pre-granulosa cells. Upon activation, these cells grow into a single layer of cuboidal cells in the PF. Further proliferation of the granulosa cells results in the formation of two or more layers and is accompanied by oocyte growth; these follicles can be identified as SF (Fair *et al.*, 1997, Monferini *et al.*, 2024).

Furthermore, the PMF, PF, and SF transcriptome analyses, as evidenced by sequencing studies in humans, primates, and mice (Chen *et al.*, 2022, Wang *et al.*, 2020a, Zhang *et al.*, 2018), have characterized the molecular profiles of individual categories of preantral follicles. Effective culture systems should cater to the distinct properties of these three follicle categories. Targeted systems have been successful in culturing follicles from the large SF stage (Araújo *et al.*, 2015, da Cunha *et al.*, 2018, Passos *et al.*, 2013, Paulino *et al.*, 2020, Paulino *et al.*, 2018). Fewer have attempted to culture small SF (Zoheir *et al.*, 2017) and PF (Hulshof *et al.*, 1995, Sun and Li, 2013), while isolated PMF culture remains under investigation (Dey *et al.*, 2024b).

Isolated culture systems show that PMF die quickly after a short period, regardless of the culture method or the system's dimensionality (Abir *et al.*, 2001, Abir *et al.*, 1999, Hovatta *et al.*, 1999).

While understanding the factors necessary for the growth and development of follicles to the following stages is essential to effectively improve current culture systems, it is equally vital to comprehend the reasons and mechanisms behind follicle death. Ovarian follicles experience atresia through various programmed cell death (PCD) processes throughout mammalian life, beginning *in utero* with establishing the ovarian reserve, involving mechanisms such as apoptosis, autophagy, ferroptosis, necroptosis, etc. (Chaudhary *et al.*, 2019a, Chaudhary *et al.*, 2019b, Grive, 2020, Sun *et al.*, 2020). Postnatally, integrated stress response genes have been found to play a key role in determining the fate of dormant PMF between attrition and activation (Cari *et al.*, 2021). Although many other modes of PCD have been identified as active in the ovary over the years (Grive, 2020), we hypothesize that the isolated PMF may undergo one or more forms of PCD after a brief period in culture. Our primary goal is to clarify which PCD mechanisms contribute to follicle death during culture at different time points in a serum-free 2D culture system. These pathways can be inhibited to improve current PMF culture systems and enhance ARTs.

This study employs a top-down approach to interrogate the follicles to understand their survival necessities. We accomplished this by comparing the transcriptome profiles of freshly isolated versus cultured PMF, identifying highly connected genes (hub genes) that are potentially decisive in regulating PMF fate *in vitro*. The transcriptome analysis further informed the appropriate supplementation with glycine, which regulates lipid peroxidation and intercepts the ferroptosis

cascade, thereby ameliorating the culture system and enhancing PMF survival *in vitro*.

Materials and Methods

Ethics Statement

All the experiments were carried out using bovine ovaries collected at the abattoir (INALCA SpA, Ospedaletto Lodigiano, LO, Italy, IT 2270M CE) following the specific health requirements. No animals were raised or killed purposely to collect ovaries. The ovaries used to collect the follicles employed for the experiments are discarded by-products of the food industry, which produces meat for human consumption. As such, we fulfilled the 3Rs principles (Replacement, Reduction, and Refinement) by reusing leftover organs as abattoir waste.

Materials

Unless stated otherwise, all chemicals and reagents used in this study were obtained from Merck Sigma Aldrich, Milan, Italy. Disposable sterile plasticware was purchased from SARSTEDT Srl, Trezzano sul Naviglio, Italy (SARSTEDT Green line for suspension cells) and Thermo Fisher Scientific Inc, Monza, Italy (NUNC IVF Line and Sterilin™). Unless specified otherwise, all procedures were conducted at room temperature (26 °C).

Primordial Follicle Isolation and Culture

Holstein Friesian heifers were used as an experimental model to maximize the number of PMF released per mm^3 of the ovarian cortex (Monferini *et al.*, 2024). Holstein Friesian ovaries were collected from heifers aged 12 to 24 months at a local abattoir, which underwent routine veterinary inspections according to the specific health requirements. As previously described (Dey *et al.*, 2024a, Monferini *et al.*, 2024), only animals with both ovaries carrying more than 10 medium antral follicles (2-8 mm) visible on the ovarian surface were considered (Modina *et al.*, 2014). Pairs of ovaries were separated from the surrounding fat tissue and ligaments and transferred into a 50 mL tube containing sterile saline (NaCl, 9 g/L), supplemented with 100 U/mL of penicillin and 0.1 mg/mL of streptomycin (pen/strep). Ovaries were transported to the laboratory at 4°C within 1 hour and kept cool until processing to minimize ovarian tissue damage (Duncan *et al.*, 2016, Vilela *et al.*, 2021).

PMF were mechanically isolated following the previously defined protocol (Dey *et al.*, 2024a, Monferini *et al.*, 2024). Briefly, a strip measuring 10×20 mm and 0.5–1 mm thick (between 0.1 and 0.2 cm^3) was peeled off the surface of the ovarian cortex. The cortical tissue was chopped into smaller fragments using 1.5-inch single-edge razor blades, minced, and washed in 3 mL of isolation medium, which consisted of Leibovitz's L-15 Medium supplemented with 3 mg/mL Bovine Serum Albumin (BSA) and pen/strep (isolation medium). The washed minced pieces were then transferred to a 50 mL tube containing 15 mL of isolation medium. This tube was then placed under an IKA ULTRA-TURRAX® T25 Homogenizer (IKA-Werke, Staufen, Germany) equipped with the Dispersing Tool S25D-14G-KS (IKA-Werke), and the minced cortical pieces were homogenized at 3000 rpm for 6 minutes. The homogenate was

passed through a 300 µm mesh size strainer (pluriSelect Life Science, Leipzig, Germany) positioned over a 50 mL tube, with each strainer mesh washed using 5 mL of isolation medium. The filtrate was then serially passed through 100, 70, 40, and 30 µm mesh size strainers placed atop a 50 mL tube, with each strainer washed with 5 mL of isolation medium. The 30 µm strainer was flipped upside-down, stably hovered over a 60 mm Petri dish, and washed with the isolation medium to liberate the clear population of PMF. PMF were then collected under a high-zoom ratio stereomicroscope (Nikon SMZ1270i, Nikon, Tokyo, Japan) equipped with a DSFi3 camera and NIS Elements L image analysis software (Nikon). The isolation process was conducted quickly, not exceeding 40 minutes, to prevent the follicles from becoming sticky (Converse *et al.*, 2022, Dey *et al.*, 2024a, McDonnell *et al.*, 2022, Monferini *et al.*, 2024).

To recover from the stress of the procedure (Converse *et al.*, 2022), the isolated follicles were placed for 1 hour in a 4-well plate in 500 µL of culture medium as previously defined (Dey *et al.*, 2024a). The medium consisted of αMEM supplemented with 0.1% fatty-acid free BSA, ITS (1 mg/mL r-hInsulin, 0.55 mg/mL hTransferrin, 0.5 µg/mL Sodium Selenite), 10^{-4} IU/mL r-hFSH (Gonal-F, Merck Darmstadt, Germany), 0.164 mM Penicillin, and 0.048 mM Streptomycin.

Subsequently, PMF were randomly assigned to three treatment groups: PMF T0 (freshly collected after 1 hour of recovery, control), PMF T16 cultured for 16 hours, and PMF T24 cultured for 24 hours in the previously defined culture medium.

Viability Assessment

The viability of all isolated PMF at T0, T16, and T24 was assessed using a dual-fluorescence viability assay with Propidium Iodide (PI) and Fluorescein Diacetate (FDA), each diluted to a final concentration of 1 µg/mL in PolyVinyl Alcohol dissolved in Phosphate Buffer Saline at a final concentration of 0.1% (PBS/PVA, manipulation buffer) (Dey *et al.*, 2024a). Groups of follicles were washed in a 50 µL drop of manipulation buffer and then transferred to a 50 µL drop of the dual staining solution. After one minute of incubation, follicles were observed at appropriate wavelengths under a fluorescence microscope (Nikon Diaphot-TMD Inverted Microscope with fluorescent filter DM 510) equipped with a Nikon DS-L1 camera for digital image acquisition. Follicles were classified as viable when the oocyte and all the granulosa cells were alive (green fluorescence) or when there were less than 10% of dead granulosa cells (red fluorescence) (Dolmans *et al.*, 2006, Monferini *et al.*, 2024).

RNA Extraction and Sequencing

To analyze the gene expression profiles, PMF isolated as described above (three biological replicates) were retrieved and pooled after collection (T0) or 16 h of culture (T16) for RNA extraction and sequencing. Individual replicates were collected in minimum volumes of 0.1% PBS/PVA and stored in 2 mL RNAse-free tubes containing RNA lysis buffer at −80 °C until RNA extraction.

Total RNA was extracted using the miRNeasy Tissue/Cells Advanced Micro Kit (Qiagen Srl, Milan, Italy) and eluted in RNAse-free water following the manufacturer's instructions. RNA samples were processed at the Centre of Genomic Regulation, Barcelona, Spain, for library preparation and sequencing.

cDNA was generated using SMART-Seq v4 Ultra Low Input RNA kit (Clontech, Takara Bio, Saint-Germain-en-Laye, France). Briefly, first-strand cDNA synthesis was primed by the 3' SMART-Seq CDS Primer II A and uses the SMART-Seq v4 Oligonucleotide for template switching at the 5' end of the transcript. cDNA amplification was performed by LD PCR using PCR Primer II A cDNA from the SMART sequences introduced by 3' SMART-Seq CDS Primer II A and the SMART-Seq v4 Oligonucleotide. cDNA was analyzed with Agilent Bioanalyzer (Agilent Technologies Spain, S.L., Madrid, Spain) to determine the concentration. From the cDNA obtained, libraries were prepared using NEBNext® Ultra DNA Library Prep Kit for Illumina® (Ipswich, MA, USA) according to the manufacturer's protocol. Briefly, 5 ng of cDNA were fragmented at a range size of 200-500bp using Covaris S2, then subjected to end repair and addition of "A" bases to 3′ ends, ligation of NEB adapter, and USER excision. All purification steps were performed using AgenCourt AMPure XP beads (Beckman Coulter, Barcelona, Spain).

Library amplification was performed by PCR using NEBNext Multiplex Oligos for Illumina (96 Unique Dual Index Primer Pairs, Ref. E6440, E6442, E6444, E6446). To estimate the quantity, final libraries were analyzed using Agilent Bioanalyzer or Fragment Analyzer High Sensitivity assay. They were then quantified by qPCR using the KAPA Library Quantification Kit (KapaBiosystems). Libraries were sequenced on Illumina's NextSeq2000, generating 50 bp paired-end reads.

Transcriptome Analysis

Raw data were obtained and read quality was assessed using FastQC. Trimming of the reads was performed to remove artificial constructs like adapters, primers, and overcalled polyG sequences with TrimGalore and Fastp. Trimmed reads were mapped to the bovine transcriptome assembly, ARS UCD1.3, and quantified using Salmon (Patro *et al.*, 2017). The DESeq2 (Love *et al.*, 2014) package in Bioconductor/R was used to detect differentially expressed genes (DEGs) between PMF T16 and T0, and genes with False Discovery Rate (FDR) <0.1 obtained through Benjamini-Hochberg correction were considered statistically significant. The threshold was cutoff at FDR < 0.1 to broaden the exploration of enriched pathways and capture a wider range of potential network interactions. Principal component analysis of all replicates was performed with the pcaExplorer (Marini and Binder, 2019) package in R. The volcano plot and heatmap were generated with EnhancedVolcano and pHeatmap packages in R, respectively (Blighe K, 2023, Kolde, 2012).

Raw and processed data are deposited in the Gene Expression Omnibus (GEO) from NCBI and are accessible through GEO accession number GSE283263.

Over Representation Analyses

Over Representation analyses (ORA) were performed with WebGeStalt (Liao *et al.*, 2019) using gene ontology (GO) for biological function and the KEGG database for pathway. ORA of the DEGs were performed against the *Bos taurus*

species, and genome protein coding was set as the reference gene list. The minimum and maximum number of IDs in the category were set to 2 and 2000, respectively. Benjamini-Hochberg correction was used for multiple test adjustments. Biological processes and KEGG pathways with a False Discovery Rate (FDR) < 0.1 were considered significant. Overrepresented biological processes and pathways were plotted with the ggplot2 package in R.

Network Analysis

The network of DEGs was constructed through the GeneMANIA plugin (Montojo *et al.*, 2010) on Cytoscape version 3.9.1 (Otasek *et al.*, 2019). The association data employed was genetic or physical interaction. The network was generated against *Homo sapiens*, with 0 additional related genes and, at most, 10 attributes with the default automatic selected weighting method (Mostafavi *et al.*, 2008, Warde-Farley *et al.*, 2010).

Hub Gene Identification

The network node (gene) scores were calculated with the cytoHubba plugin, which offers different node ranking methods to evaluate the importance of genes (nodes) in a biological network (Chin *et al.*, 2014). Two topological analysis methods (local-based) and 4 typical centrality parameters (global-based) for networks were employed to generate subnetworks of the top 20 highly connected hub genes according to each method i.e., Degree, Maximum Neighborhood Component (MNC), Betweenness, Closeness, Radiality and Stress.

The 6 subnetworks were merged by intersection to identify the common hub genes across all the subnetworks. Genes in the merged network were identified as central hub genes and were color-coded as per their log_2FoldChange (log_2FC) values at PMF T16, i.e., upregulated DEGs ($log_2FC \geq 0.5$) were color-coded green and downregulated DEGs ($log_2FC \leq -0.5$) were color-coded red. A circular layout was adopted to visualize the central hub gene network. Gene ontologies of the central hub genes concerning biological processes and molecular functions were obtained from UniProtKB.

Investigation of Different Programmed Cell Death Mechanisms

Four main PCD occurrences were investigated: apoptosis, autophagy, ferroptosis, and necroptosis. Information about the genes and signaling network regulating the four PCD mechanisms was downloaded from publicly available databases. Apoptosis: Deathbase (http://deathbase.org/) (Díez *et al.*, 2010),

Autophagy: HADb (http://autophagy.lu/) (Moussay *et al.*, 2011), Ferroptosis: FerrDbv2 (http://www.zhounan.org/ferrdb/current/) (Zhou *et al.*, 2023b), and Necroptosis: KEGG (https://www.genome.jp/entry/pathway+bta04217) (Kanehisa, 2000, Kanehisa, 2019, Kanehisa *et al.*, 2023). The KEGG Necroptosis pathway was obtained since no dedicated database for necroptosis was found.

The UpSet plot was constructed with the ComplexUpset (Krassowski, 2020, Lex, 2014) package in R to allocate the number of DEGs in our dataset involved in 4 main PCD mechanisms, i.e., apoptosis, autophagy, ferroptosis, and necroptosis. Chi-square tests were conducted to confirm the significance of the association between genes shared between the individual mechanisms and the list of DEGs. A $p < 0.01$ was considered significant and confirmative of association.

To functionally categorize the ferroptosis genes found, a list of genes related to ferroptosis was obtained from FerrDbv2 (Zhou *et al.*, 2023b). A Venn diagram was constructed with the VennDiagram package (Chen and Boutros, 2011) in R to identify ferroptosis drivers and suppressors that were differentially expressed between PMF T16 vs T0. Each gene on FerrDbv2 is assigned a score, classifying it as either a driver or suppressor. DEGs identified as having a dual role, i.e., both drivers and suppressors were reclassified according to their score on FerrDbv2, so DEGs that scored higher as drivers were reclassified as ferroptosis drivers, and those scored higher as suppressors were reclassified as ferroptosis suppressors.

Ferroptosis DEG Network Generation

The interaction data of the ferroptosis DEGs, classified into drivers and suppressors, were downloaded from FerrDbv2 and imported into Cytoscape. The interaction data were then used to generate the directed (Driver/Suppressor) network.

Glycine Supplementation and Viability Assessment

As revealed by our transcriptome analysis, we aimed to ameliorate our defined culture medium by adding glycine to suppress ferroptosis. Previous studies demonstrated that 6 mM glycine supplementation effectively reduced the occurrence of ferroptosis by increasing glutathione (GSH) in *in vitro* matured porcine oocytes (Gao *et al.*, 2023). Therefore, we conducted experiments on isolated PMF using the same glycine concentration. This experiment was designed as a proof-of-principle to demonstrate the involvement of glycine in suppressing ferroptosis.

Isolated PMF were cultured for 16 h in the previously defined culture system supplemented with 6 mM glycine. Viability staining with PI/FDA was performed as described before.

Statistical analysis

Statistical analysis of the viability assessments was conducted using GraphPad PRISM version 10.1.1 (GraphPad Software, Boston, MA, USA, www.graphpad.com). Experiments were replicated five times. Normality tests were run to assess normal data distribution. Data were analyzed by one-way ANOVA followed by Tukey's multiple comparisons test, and values were reported as mean percentage ± SEM. Significant differences were defined at $p < 0.05$.

Results

Viability Assessment

Approximately 90% (88.99 ± 2.99%) of isolated PMF were viable at T0 as assessed by PI/FDA dual staining (Figure 1). Following 16 h of culture (T16), viability was found to be 69.46 ± 3.18 % and 64.61 ± 3.34 % after 24 h (T24). The decline in viability was significant after 16 h ($p = 0.0003$) and 24 h of culture ($p \leq 0.0001$). In contrast, the decrease observed between 16 h and 24 h was limited and not statistically significant.

The present experiment identified the timeframe in which programmed cell death may occur, specifically within 0 to 16 h of culture. As a result, separate experiments were conducted to profile the transcriptomes of PMF at T0 and T16, aiming to understand which PCD mechanisms may have triggered the decline in PMF viability.

RNA Sequencing and Transcriptome Analysis

Table 1 defines the number of follicles in each replicate submitted for RNA extraction and sequencing. The mapping rate was between 87% and 92% for all the samples.

Principal component analysis (PCA) showed apparent clustering of PMF at T0 versus T16 with ~38% variance between the groups along the first component (PC1) as shown in (Figure 2A). Differential gene expression analysis revealed 1949 DEGs (FDR < 0.1) between PMF at T16 versus at T0 (Figure 2B, Supplementary Table S1). The heatmap of the top 50 most variable genes in (Figure 2C) shows the expression profile at the two time points.

Over Representation Analyses

ORA showed functional enrichment of biological processes such as positive regulator of cell death, negative regulator of cell proliferation, growth, and response to cytokines (Figure 3A). Overrepresented KEGG pathways included TNF and MAPK signaling pathways and glycine, serine, and threonine metabolism, as shown in (Figure 3B).

Hub Gene Identification

Upon merging the top 20 hub genes in each of the 6 centrality measure subnetworks (Supplementary Figure S1), 14 genes were found to be common across all 6 subnetworks, namely, *Solute Carrier Family 7 Member 11* (*SLC7A11*), *DNA Topoisomerase 1* (*TOP1*), *Baculoviral IAP Repeat-Containing Protein 3* (*BIRC3*), *Ubiquitine-protein ligase 3A* (*UBE3A*), *POU domain class 3 transcription factor 3* (*POU3F3*), *neurotrophic receptor tyrosine kinase 3* (*NTRK3*), *Glypican 5* (*GPC5*), *Contactin 4* (*CNTN4*), *Sorbin and SH3 domain-containing protein 2* (*SORBS2*), *MDS1 And EVI1 Complex Locus* (*MECOM*), *Receptor-Type Tyrosine-Protein Phosphatase Delta* (*PTPRD*), *Receptor-Type Tyrosine-Protein Phosphatase Mu* (*PTPRM*), *Estrogen Receptor 1* (*ESR1*) and *Transcription Factor Jun* (*JUN*) (Figure 4). These were identified as the common hub genes of the merged network that may play an essential role in regulating PMF gene expression, biological processes, and molecular functions (Supplementary Table S2).

Investigation of Different Programmed Cell Death Mechanisms

From the analysis, 45 DEGs were found to be involved in ferroptosis, 19 in autophagy, 12 necroptosis, and 8 in apoptosis, as depicted in (Figure 5A). Identified DEGs related to each PCD and their $\log_2$FC values have been listed in the Supplementary Table S3. The chi-square test confirmed the association of the DEGs with prespecified ferroptosis (p = 9.9E-12) and autophagy (p = 3.9E-07) pathway genes. At the same time, no association was determined between the DEGs and necroptosis and apoptosis.

Of the 45 ferroptosis genes identified to be differentially expressed in our data, (Figure 5B) shows that 21 DEGs were found to be ferroptosis drivers, 23 were classified as ferroptosis suppressors, and 1, *PIK3CA* was found to have a dual function as listed on FerrDBv2.

The directed network shows the molecular regulation concerning ferroptosis that occurs in the PMF at 16 h of culture (Figure 5C). DEGs and their signaling pathways involved in ferroptosis are graphed. At this point, while many DEGs are driving ferroptosis like *KDM5C*, lipid ROS formation like *ACSL4*, and driving an integrated stress response (ISR), others are upregulating ferroptosis suppressors such as *SLC7A11* and *CAV1* and inhibiting lipid ROS formation like *SESN2*. Therefore, the differential expression of drivers and suppressors in the network captured at T16 in the network in (Figure 5C) demonstrates that at this precise point in the culture period, the cells are still actively responding to ferroptosis inducers, and they are not fully committed to cell death yet.

Glycine Supplementation and Viability Assessment

As in the previous experiment, approximately 90% of isolated PMF (87.51 ± 2.22%) were viable at T0. Again, following 16 h of culture, the viability of isolated PMF cultured without glycine (T16) was significantly lower than at T0 at 76.97 ± 2.64% ($p = 0.0041$). However, isolated PMF cultured for 16 h in a glycine supplemented medium (T16 Gly) showed a significant higher viability (84.66 ± 1.51%) compared to PMF T16 ($p = 0.0433$) and not significantly different from that of PMF at T0 (Figure 6).

Discussion

Current ARTs are limited in fully exploiting the most abundant part of the mammalian ovarian reserve, the PMF, since no *in vitro* culture system can entirely support isolated PMF's long-term development into mature gametes (Abir *et al.*, 1999, Hornick *et al.*, 2012). The shortcoming of isolated PMF *in vitro* culture is likely due to the lack of knowledge of the events guiding these follicles to develop into PF *in vivo* (McGee and Hsueh, 2000) and the challenges connected with their manipulation.

Regardless of dimensionality, *in vitro* culture of isolated preantral follicles has shown some success beginning from the large SF stage (Araujo *et al.*, 2014, McLaughlin *et al.*, 2010), while PMF degenerate after a short culture period (Abir *et al.*, 2001, Abir *et al.*, 1999, Hovatta *et al.*, 1999). To design a system capable of growing PMF to PF *in vitro*, it is essential to understand the mechanisms guiding their transition to the PF stage and why these follicles die upon isolation. The present study mainly focuses on answering the latter question by investigating the early changes in expression profile to reveal the mechanisms governing the fate of PMF in a defined culture system. The molecular underpinnings of PMF survival *in vitro* would allow the development of an efficient and effective culture system.

The present study shows that approximately 90% of PMF were viable at T0, a percentage higher than previous reports of mechanical isolation methods in bovine species (Langbeen *et al.*, 2015). We show that after 16 h of culture, although the viability declines by about 30%, the viable PMF remains above 60% until 24 h of culture. Within this window of opportunity, we used the earlier time point to visualize the genomic regulation activated in the PMF by isolation from the ovarian stroma and

early steps of *in vitro* culture to understand the cause of PMF death *in vitro*. This informed the appropriate medium supplementation with glycine, achieving about 85% PMF viability for 16 h in a defined 2D culture system. Previous studies on isolated primordial follicle culture in humans and rhesus macaques used different isolation methods (mechanical or enzymatic), degrees of isolation (fully or partially isolated), and dimensionality of the culture system (on or within collagen or alginate gels) in serum-supplemented medium (Abir *et al.*, 2001, Abir *et al.*, 1999, Hornick *et al.*, 2012, Hovatta *et al.*, 1999). These studies differ from the approach presented here, limiting direct comparisons.

Nevertheless, previous reports indicate that fully isolated human PMF cultured on various matrices deteriorate rapidly within 24 hours (Abir *et al.*, 2001), and rhesus macaque PMF, in the absence of any biomaterial encapsulation, dissociate by 3 days of culture (Hornick *et al.*, 2012). Thus, our glycine-supplemented culture system demonstrates progress compared to earlier studies. Moreover, we implemented a different strategy through RNA-seq analysis to dissect the molecular events triggered during PMF culture. These data should guide future research on ex-vivo growth and PMF development in higher-scale mammals.

By comparing the transcriptome landscape of the two follicle groups, we identified 1949 DEGs that, according to functionally enriched key GO biological processes and KEGG pathways, are substantially involved in cell proliferation and death. Both the MAPK and TNF signaling pathways are known to play a role in cell fate determination, as well as in primordial follicle activation *in vivo* (Chen *et al.*, 2020, Greenfeld *et al.*, 2007, Li-Ping *et al.*, 2010, Silva *et al.*, 2020, Wright *et al.*, 2020, Zhao *et al.*, 2018). However, they also have a dual role in promoting PCD. For instance, MAPK is one of the most potent classical inflammatory signaling pathways

linked to pro-inflammatory cell death pathways like necroptosis, ferroptosis, and pyroptosis, in addition to apoptosis and autophagy, which are generally considered non-inflammatory (Chen *et al.*, 2023, Ikeda *et al.*, 2019, Kolb *et al.*, 2017, Van Loo and Bertrand, 2023, Wang *et al.*, 2023). Likewise, the TNF signaling pathway is associated with necroptosis and pyroptosis (Li *et al.*, 2014, Samson *et al.*, 2021, Tanzer, 2022, Van Loo and Bertrand, 2023, Wang *et al.*, 2020b) and suppresses ferroptosis through the synthesis of GSH (Wu *et al.*, 2022), which occurs through the amino acid antiporter system genes, *SLC7A11* - identified as a common hub gene - and *SLC3A2*, components of the System X_c^-.

While PMF activation and the processes guiding PMF-to-PF transition are yet to be fully resolved, we noted the differential expression of some previously studied essential genes. Key cell cycle inhibitor genes such as *CDKN1B* (also known as p27), *CDKN2B* (Frost *et al.*, 2022, Zhang *et al.*, 2023), and TGF-β signaling pathway genes (Patton *et al.*, 2021, Zhang *et al.*, 2023) were found to be differentially expressed in this study. Previous reports have shown that the TGF-β signaling pathway has a role in maintaining PMF dormancy (Wang *et al.*, 2014). The transcription factor, *SMAD3*, a signaling mediator of the TGF-β, reported to be expressed in the pre-granulosa cells of mice PMF (Granados-Aparici *et al.*, 2019), was found to be upregulated at T16 along with *TGFBRAP1*, *TGFB2*, and its corresponding receptor, *TGFBR2*. Furthermore, a scRNA-seq study in mice reported a cluster of signature genes to either be switched on or off in PMF activation. In line with the study, we identified *H19* to be switched off in PMF T16 (Frost *et al.*, 2022). Additionally, *TAC1* has been reported to be expressed during the PMF-to-PF transition in mice (Bernabé *et al.*, 2020), and an upregulation of the gene was found in the PMF T16. Since the PMF compartments were not sequenced separately, this

study cannot trace whether transcripts were expressed in the oocyte or pre-granulosa cells, limiting further insight. Nevertheless, collectively, the expression of these genes aligns with those previously reported in the literature, albeit in different species, suggesting that isolated PMF may be attempting to positively regulate the development of PF in the provided culture system. While individually, these genes offer molecular cues to assess the culture system, rigorous studies of healthy PMF and PF genomic regulations are needed to clarify their role in bovine preantral folliculogenesis and optimize the system accordingly.

The hub gene analysis identified 14 genes through six common centrality algorithms as central hub genes influencing the downstream processes in the PMF. Key transcription factors, *JUN*, *POU3F3*, and *ESR1*, were all downregulated. Pharmacological inhibition of c-JUN phosphorylation in ovine ovarian cortex culture has been shown to inhibit PMF activation *in situ* (Bertoldo *et al.*, 2016). The present analysis further revealed genes involved in PCD, specifically in ferroptosis, such as *SLC7A11*, a well-known ferroptosis suppressor (Koppula *et al.*, 2021). Additionally, *NTRK3*, which is involved in maintaining oocyte viability during the PMF-to-PF transition, was found to be downregulated at T16 (Nilsson *et al.*, 2009).

Given the many DEGs involved in ferroptosis (Figures 4 and 5) compared to autophagy and their broader spectrum of fold change (Supplementary Table S3) between the two time points, ferroptosis may be considered the primary PCD mechanism involved. This finding implies that ferroptosis may be the leading PCD mechanism causing the death of PMF within the 16 h window.

The 16 h culture period offers insight into the molecular functioning of the PMF at that time point. In other words, the central hub gene network captures the probable decision-making process of the PMF at T16. At this time point, the upregulation of

546 *SLC7A11* is both influencing and being influenced by the expression of the
547 remaining 13 central hub genes, such as *JUN* and *ESR1*. These central hub genes
548 are well-known transcription factors that play roles in cell differentiation and
549 proliferation and are involved in signaling pathways such as NF-kappaB
550 (Oeckinghaus *et al.*, 2011) and estrogen signaling pathways (Fuentes and Silveyra,
551 2019, Lung *et al.*, 2020, Marino *et al.*, 2006). The PMF at T16 have already launched
552 a defense response to ferroptosis and have switched into survival mode instead of
553 allowing follicle activation, i.e., most evidently, by the lack of pre-granulosa cell
554 proliferation into granulosa cells and PF formation *in vitro*. Additionally, *BIRC3*,
555 *TOP1*, and *UBE3A* are upregulated at T16 and are responsible for inhibiting other
556 PCD mechanisms like apoptosis and necroptosis, regulating DNA replication,
557 transcription, and repair, while also coordinating ubiquitin-mediated protein
558 degradation within cells, respectively (Supplementary Table S2).
559 Broadly, molecular chaperones, like heat shock proteins, interact with other
560 proteins to prevent their degradation and ensure proper protein folding, thereby
561 assisting in maintaining cell homeostasis. The differential gene expression analysis
562 also identified heat shock proteins belonging to the HSP70 and HSP110 family
563 proteins (Liu *et al.*, 2022) – *HSPA12A*, *HSPA14*, *HSPA9*, and *HSPH1*, respectively –
564 all of which were upregulated at PMF T16. Previous reports suggest that *HSPH1*
565 plays a protective role against lipid peroxidation during ferroptosis by binding to and
566 stabilizing *SLC7A11* (Xu *et al.*, 2023). PCD mechanisms today canopy a wide
567 assortment of ‘ptosis’, and since the first report of apoptosis in 1947, is ever
568 expansive (Dey and Luciano, 2022). Ferroptosis is uniquely characterized as an iron-
569 dependent form of non-apoptotic cell death. Its occurrence in female reproduction
570 has since been investigated across diverse physiological conditions, including but

not limited to diminished ovarian reserves in women with advanced maternal age (Jia *et al.*, 2023), PMF depletion in obese mice (Zhou *et al.*, 2023a), and the pathogenesis of polycystic ovarian syndrome (Tan *et al.*, 2022). Impaired *In vitro* oocyte maturation and decreased oocyte quality have been linked to iron overload-induced ferroptosis in porcine (Hu *et al.*, 2021).

On the other hand, glycine, an essential component of GSH synthesis, has been shown to promote *in vitro* porcine oocyte maturation and early embryonic development by reducing the occurrence of ferroptosis when supplemented exogenously (Gao *et al.*, 2023, Zhang *et al.*, 2024). This protective effect is mediated through the ferroptosis surveillance mechanism involving the cystine/glutamate antiporter (System X_c^-), GSH, and glutathione peroxidase 4 (GPX4)—collectively known as the System X_c^-/GSH/GPX4 axis (Chen *et al.*, 2021, Jiang *et al.*, 2021, Jiang *et al.*, 2024, Li *et al.*, 2022). In line with these findings, our analysis also revealed a significant over-representation of glycine, serine, and threonine metabolism (Figure 3B). Therefore, we supplemented our defined medium with glycine to potentially rescue PMF from ferroptosis. The glycine-supplemented culture medium was then able to sustain PMF viability at about 85% for 16 h, approximately 25% higher than that of PMF cultured without glycine. Hence, our redefined medium enhanced PMF viability in culture for up to 16 h and, with further examination of viability at later time points, may offer an extended window for studying isolated PMF genomic regulation *in vitro*. Additionally, an in-depth investigation into the mechanism of glycine rescue may help clarify whether ferroptosis suppression is linked to the observed increase in PMF viability.

Merely suppressing PCD in culture systems may not necessarily be sufficient to promote quality-intact follicle development. A combination of supplements may

need to be tested to prevent PMF death, sustain quiescence, and trigger activation throughout the culture period (Pargianas *et al.*, 2020). Vitamin E, specifically α-tocopherol hydroquinone, acts as an inhibitor of ferroptosis (Hinman *et al.*, 2018, Zeng *et al.*, 2025). Alpha-tocopherol has been tested for its antioxidant properties in the *in situ* culture of caprine PMF. While an increase in PMF activation was observed, it was accompanied by an overall reduction in follicle viability after culture (Lima-Verde *et al.*, 2009, Lucia Dos Santos Silva *et al.*, 2023). Consequently, when establishing a microenvironment to culture PMF, it is essential to add ferroptosis inhibitors to the culture medium to prevent them from entering fight or flight mode and also to supplement the system with necessary activators or enhancers of cell proliferation and development to direct them towards PMF activation and subsequent PF development.

As such, deeper analyses of the PMF-to-PF transition in isolated bovine follicles need to be conducted, followed by additional supplement testing to optimize the current culture system (Pargianas *et al.*, 2020). This study is limited to the PCD mechanisms responsible for isolated PMF death in a serum-free 2D culture method and the rescue strategy informed by these mechanisms. Studies have suggested the biomechanical role of the rigid ovarian cortex in maintaining the quiescence of PMF through inhibitory signals (Fiorentino *et al.*, 2022, Méndez *et al.*, 2022) and nuclear rotation of the oocyte (Nagamatsu *et al.*, 2019). We speculate that understanding the mechanism of these signals will allow for the sustained viability of isolated PMF *in vitro* before timely activation and development into PF, which may be permitted by a precisely tuned culture system. Therefore, future physiological culture systems should aim to synchronize the dynamic modulation of these molecular signals to

effectively supplement the media and enhance the recapitulation of the PMF-to-PF transition *in vitro.*

In conclusion, our study suggests that ferroptosis plays a role in inducing isolated PMF death in a serum-free 2D culture system, likely suppressed with glycine to improve the *in vitro* follicle culture system. The outcome of this analysis is expected to provide new strategies for fertility preservation through early intervention. Potential applications include saving endangered species, enhancing livestock breeding and selection schemes, and increasing the likelihood of fertility treatments for women with advanced maternal age, premature ovarian insufficiency, polycystic ovary syndrome, or other infertility issues. For women and young girls battling cancer, chemotherapeutic treatments often diminish the ovarian reserve. If PMF can be rescued from a small tissue fragment before the oncotherapy and appropriate culture systems can support their development, a safe option for future conception may be available for these patients.

Data Availability

Raw and processed data are deposited in the Gene Expression Omnibus (GEO) from NCBI and are accessible through GEO accession number GSE283263.

Acknowledgments

The authors thank INALCA S.p.A. (Ospedaletto Lodigiano, LO), Mr. Gianluca Pesatori, Dr. Massimo Sinelli, and the veterinary staff for their valuable support. The authors also thank Dr. Paola Cremonesi, IBBA-CNR, Lodi, for assistance with the Bioanalyzer and Dr. Irene González Navarrete of the Genomics Unit at the Centre for Genomic Regulation, Barcelona, for assistance with the sequencing.

Authors' roles

P.D. and A.M.L. conceived the idea and designed the study. P.D., N.M., L.D., and A.M.L. performed the experiments. P.D., N.M., V.L., F.F., F.Z., and A.M.L. were involved in RNA extraction and sequencing. F.Z., M.B.R., and F.F. collaborated on the data analysis and visualization performed by P.D.. P.D. drafted the manuscript, which was revised by A.M.L. All authors critically discussed the results and contributed to the final manuscript.

Funding

This project has received funding from the European Union's Horizon 2020 research and innovation programme under the Marie Skłodowska-Curie grant agreement No. 860960 ("EUROVA"), and was supported by Regione Lombardia FEASR - Programma di Sviluppo Rurale 2014-2020, Sottomisura 10.2 – "Sostegno per la conservazione, l'uso e lo sviluppo sostenibili delle risorse genetiche in agricoltura" - Operazione 10.2.01 – "Conservazione della biodiversità animale e vegetale" No. 202102146691 (R-INNOVA), and by the Italian Ministry of University and Research (MUR), PRIN2020, No. 20209L8BN4 (InfinitEGG).

PD fellowship is supported by funding from the European Union's Horizon 2020 Marie Skłodowska-Curie Innovative Training Network, grant agreement No. 860960 ("EUROVA"). NM doctoral scholarship was co-funded with resources in the frame of the PON REACT-EU financing Program Action IV.5 – Doctorates on green topics.

Conflict of Interest

The authors have no conflicts of interest to declare.

Figure Legends

Figure 1. Viability assessment of freshly collected and *in vitro* cultured primordial follicles. (A) Viability assessment of PMF T0 and PMF T16 using PI and FDA. Scale bar = 100 µm. (B) Viability of PMF after 0, 16, and 24 h of culture, T0 (N= 311), T16 (N=175), and T24 (N=199), respectively. The experiment was repeated 5

680 times (n=5). Data were analyzed by one-way ANOVA followed by Tukey's multiple
681 comparisons test, and values were reported as mean percentage ± SEM. **** indicate
682 significant differences between groups where p ≤0.0001, *** indicate significant
683 differences between groups where p<0.005; ns: not significant. PMF T0, freshly
684 collected primordial follicles, control; PMF T16, primordial follicles cultured for 16 h;
685 PMF T24, primordial follicles cultured for 24 h; PI, Propidium Iodide; FDA, Fluorescein
686 Diacetate
687
688 **Figure 2. Transcriptome analysis of freshly collected and *in vitro* cultured**
689 **primordial follicles.** (A) Principal Component Analysis (PCA) plot shows apparent
690 clustering of PMF T0 and T16. (B) Volcano plot of differential gene expression (DGE)
691 analysis shows up and downregulated DEGs (FDR<0.1) determined between PMF
692 T0 and PMF T16 represented by green and red dots, respectively. (C) Heatmap of
693 top 50 most variable genes. The heatmap shows normalized gene expression by
694 regularized log transformation. PMF T0, freshly collected primordial follicles, control;
695 PMF T16, primordial follicles cultured for 16 h; DEGs, differentially expressed genes;
696 FDR, false discovery rate
697
698 **Figure 3. Over Representation Analysis of genes differentially expressed**
699 **between freshly collected and *in vitro* cultured primordial follicles.** Over
700 Representation Analysis of 1949 DEGs shows enriched (A) GO: Biological
701 Processes. (B) KEGG pathways. The ontological terms were enriched at FDR < 0.1.
702 DEGs (FDR < 0.1) were determined between PMF T0 and PMF T16. DEGs,
703 differentially expressed genes; GO, gene ontology; FDR, false discovery rate; PMF

T0, freshly collected primordial follicles, control; PMF T16, primordial follicles cultured for 16 h

Figure 4. Hub gene identification analysis of genes differentially expressed between freshly collected and *in vitro* cultured primordial follicles. Hub gene identification analysis performed with CytoHubba identified the top 14 hub genes. Node representations: Green and red rectangles represent up and downregulated DEGs, respectively, determined between PMF T0 and PMF T16 (FDR < 0.1). DEGs, differentially expressed genes; PMF T0, freshly collected primordial follicles, control; PMF T16, primordial follicles cultured for 16 h; FDR, false discovery rate

Figure 5. Investigation of different programmed cell death mechanisms. (A) UpSet plot of DEGs determined between PMF T0 and PMF T16 (FDR < 0.1) overlapped with genes involved in ferroptosis, autophagy, necroptosis, and apoptosis. (*represents PCD mechanisms significantly associated with the DEGs (B) Venn diagram of ferroptosis drivers and suppressors differentially expressed between PMF T16 and T0. (C) Node representations: Green and red circles represent up and downregulated DEGs, respectively; grey circles represent genes not significantly differentially expressed in our dataset, and purple circles represent pathways or processes. Edge representations: Yellow lines represent inhibition, and blue lines represent activation of a gene, molecule, or pathway. DEGs, differentially expressed genes; PMF T0, freshly collected primordial follicles, control; PMF T16, primordial follicles cultured for 16 h; FDR, false discovery rate; PCD, programmed cell death

729 **Figure 6. Viability assessment of *in vitro* cultured primordial follicles**
730 **supplemented with glycine.** The graph shows the viability of PMF after 0 h and 16 h
731 of culture with 6 mM glycine, T0 (N=334), T16 (N=349), and T24 (N=368), respectively.
732 The experiment was repeated 5 times (n=5). Data were analyzed by one-way ANOVA
733 followed by Tukey's multiple comparisons test, and values were reported as mean
734 percentage ± SEM. ** indicates significant differences between groups where $p \leq$
735 0.005, * indicates significant differences between groups where $p \leq 0.05$ and ns: not
736 significant. PMF, T0, freshly collected primordial follicles, control; PMF T16, primordial
737 follicles cultured for 16 h
738

References

Abir R, Fisch B, Nitke S, Okon E, Raz A, Ben Rafael Z. Morphological study of fully and partially isolated early human follicles. *Fertil Steril* 2001;**75**:141-146.

Abir R, Roizman P, Fisch B, Nitke S, Okon E, Orvieto R, Ben Rafael Z. Pilot study of isolated early human follicles cultured in collagen gels for 24 hours. *Hum Reprod* 1999;**14**:1299-1301.

Araujo VR, Gastal MO, Figueiredo JR, Gastal EL. In vitro culture of bovine preantral follicles: a review. *Reprod Biol Endocrinol* 2014;**12**:78.

Araújo VR, Gastal MO, Wischral A, Figueiredo JR, Gastal EL. Long-term in vitro culture of bovine preantral follicles: Effect of base medium and medium replacement methods. *Anim Reprod Sci* 2015;**161**:23-31.

Bastings L, Beerendonk CC, Westphal JR, Massuger LF, Kaal SE, van Leeuwen FE, Braat DD, Peek R. Autotransplantation of cryopreserved ovarian tissue in cancer survivors and the risk of reintroducing malignancy: a systematic review. *Hum Reprod Update* 2013;**19**:483-506.

Bernabé BP, Woodruff T, Broadbelt LJ, Shea LD. Ligands, Receptors, and Transcription Factors that Mediate Inter-Cellular and Intra-Cellular Communication during Ovarian Follicle Development. *Reprod Sci* 2020;**27**:690-703.

Bertoldo MJ, Bernard J, Duffard N, Tsikis G, Alves S, Calais L, Uzbekova S, Monniaux D, Mermillod P, Locatelli Y. Inhibitors of c-Jun phosphorylation impede ovine primordial follicle activation. *Mol Hum Reprod* 2016;**22**:338-349.

Blighe K RS, Lewis M. EnhancedVolcano: Publication-ready volcano plots with enhanced colouring and labeling. 2023.

Cari EL, Hagen-Lillevik S, Giornazi A, Post M, Komar AA, Appiah L, Bitler B, Polotsky AJ, Santoro N, Kieft J *et al.* Integrated stress response control of granulosa cell translation and proliferation during normal ovarian follicle development. *Mol Hum Reprod* 2021;**27**:gaab050.

Chaudhary GR, Yadav PK, Yadav AK, Tiwari M, Gupta A, Sharma A, Pandey AN, Pandey AK, Chaube SK. Necroptosis in stressed ovary. *J Biomed Sci* 2019a;**26**:11.

Chaudhary GR, Yadav PK, Yadav AK, Tiwari M, Gupta A, Sharma A, Sahu K, Pandey AN, Pandey AK, Chaube SK. Necrosis and necroptosis in germ cell depletion from mammalian ovary. *J Cell Physiol* 2019b;**234**:8019-8027.

Chen H, Boutros PC. VennDiagram: a package for the generation of highly-customizable Venn and Euler diagrams in R. *BMC Bioinformatics* 2011;**12**:35.

Chen X, Yu C, Kang R, Kroemer G, Tang D. Cellular degradation systems in ferroptosis. *Cell Death Differ* 2021;**28**:1135-1148.

775 Chen Y-Y, Russo DD, Drake RS, Duncan FE, Shalek AK, Goods BA, Woodruff TK.
776 Single-cell transcriptomics of staged oocytes and somatic cells reveal novel regulators
777 of follicle activation. *Reproduction* 2022;**164**:55-70.

778 Chen Y, Fang Z-M, Yi X, Wei X, Jiang D-S. The interaction between ferroptosis and
779 inflammatory signaling pathways. *Cell Death Dis* 2023;**14**:205.

780 Chen Y, Yang W, Shi X, Zhang C, Song G, Huang D. The Factors and Pathways
781 Regulating the Activation of Mammalian Primordial Follicles in vivo. *Front Cell Dev Biol*
782 2020;**8**.

783 Chin C-H, Chen S-H, Wu H-H, Ho C-W, Ko M-T, Lin C-Y. cytoHubba: identifying hub
784 objects and sub-networks from complex interactome. *BMC Syst Biol* 2014;**8**:S11.

785 Converse A, Zanicker EJ, Amargant F, Duncan FE. Recapitulating folliculogenesis and
786 oogenesis outside the body: encapsulated in vitro follicle growth. *Biol Reprod*
787 2022;**108**:5-22.

788 da Cunha EV, Melo LRF, Sousa GB, Araujo VR, Vasconcelos GL, Silva AWB, Silva
789 JRV. Effect of bone morphogenetic proteins 2 and 4 on survival and development of
790 bovine secondary follicles cultured in vitro. *Theriogenology* 2018;**110**:44-51.

791 Dey P, Luciano AM. A century of programmed cell death in the ovary: a commentary.
792 *J Assist Reprod Genet* 2022;**39**:63-66.

793 Dey P, Monferini N, Donadini L, Lodde V, Franciosi F, Luciano AM. Method of Isolation
794 and In Vitro Culture of Primordial Follicles in Bovine Animal Model. In Barchi M, De
795 Felici M (eds) *Germ Cell Development. Methods in Molecular Biology*. 2024a. Springer
796 US, New York, NY, pp. 171-182.

797 Dey P, Monferini N, Donadini L, Lodde V, Franciosi F, Luciano AM. A spotlight on
798 factors influencing the in vitro folliculogenesis of isolated preantral follicles. *J Assist*
799 *Reprod Genet* 2024b;**41**:3287–3300.

800 Díez J, Walter D, Muñoz-Pinedo C, Gabaldón T. DeathBase: a database on structure,
801 evolution and function of proteins involved in apoptosis and other forms of cell death.
802 *Cell Death Differ* 2010;**17**:735-736.

803 Dolmans MM, Michaux N, Camboni A, Martinez-Madrid B, Van Langendonckt A,
804 Nottola SA, Donnez J. Evaluation of Liberase, a purified enzyme blend, for the
805 isolation of human primordial and primary ovarian follicles. *Hum Reprod* 2006;**21**:413-
806 420.

807 Duncan FE, Zelinski M, Gunn AH, Pahnke JE, O'Neill CL, Songsasen N, Woodruff RI,
808 Woodruff TK. Ovarian tissue transport to expand access to fertility preservation: from
809 animals to clinical practice. *Reproduction* 2016;**152**:R201-R210.

810 Fair T, Hulshof SCJ, Hyttel P, Greve T, Boland M. Oocyte ultrastructure in bovine
811 primordial to early tertiary follicles. *Anat Embryol* 1997;**195**:327-336.

812 Fiorentino G, Cimadomo D, Innocenti F, Soscia D, Vaiarelli A, Ubaldi FM, Gennarelli
813 G, Garagna S, Rienzi L, Zuccotti M. Biomechanical forces and signals operating in the

814 ovary during folliculogenesis and their dysregulation: implications for fertility. *Hum*
815 *Reprod Update* 2022;**29**:1-23.

816 Frost ER, Taylor G, Boeing S, Galichet C, Baker MA, Sutherland JM, Lovell-Badge R.
817 $p27^{kip1}$-dependent gene activity within granulosa cells reveals pathways relevant for
818 control of primordial follicle activation in mice. *bioRxiv* 2022:2022.2010.2024.513438.

819 Fuentes N, Silveyra P. Estrogen receptor signaling mechanisms. 2019. Elsevier, pp.
820 135-170.

821 Gao L, Zhang C, Zheng Y, Wu D, Chen X, Lan H, Zheng X, Wu H, Li S. Glycine
822 regulates lipid peroxidation promoting porcine oocyte maturation and early embryonic
823 development. *J Anim Sci* 2023;**101**.

824 Garcia Barros R, Lodde V, Franciosi F, Luciano AM. A refined culture system of
825 oocytes from early antral follicles promotes oocyte maturation and embryo
826 development in cattle. *Reproduction* 2023;**165**:221-233.

827 Gougeon A. Dynamics of follicular growth in the human: a model from preliminary
828 results. *Hum Reprod* 1986;**1**:81-87.

829 Gougeon A, Ecochard R, Thalabard JC. Age-Related Changes of the Population of
830 Human Ovarian Follicles: Increase in the Disappearance Rate of Non-Growing and
831 Early-Growing Follicles in Aging Women. *Biol Reprod* 1994;**50**:653-663.

832 Granados-Aparici S, Hardy K, Franks S, Sharum IB, Waite SL, Fenwick MA. SMAD3
833 directly regulates cell cycle genes to maintain arrest in granulosa cells of mouse
834 primordial follicles. *Sci Rep* 2019;**9**:6513.

835 Greenfeld CR, Roby KF, Pepling ME, Babus JK, Terranova PF, Flaws JA. Tumor
836 Necrosis Factor (TNF) Receptor Type 2 Is an Important Mediator of TNF alpha
837 Function in the Mouse Ovary. *Biol Reprod* 2007;**76**:224-231.

838 Grive KJ. Pathways coordinating oocyte attrition and abundance during mammalian
839 ovarian reserve establishment. *Mol Reprod Dev* 2020;**87**:843-856.

840 Grosbois J, Bailie EC, Kelsey TW, Anderson RA, Telfer EE. Spatio-temporal
841 remodelling of the composition and architecture of the human ovarian cortical
842 extracellular matrix during in vitro culture. *Hum Reprod* 2023;**38**:444-458.

843 Hansen KR, Knowlton NS, Thyer AC, Charleston JS, Soules MR, Klein NA. A new
844 model of reproductive aging: the decline in ovarian non-growing follicle number from
845 birth to menopause. *Hum Reprod* 2008;**23**:699-708.

846 Hinman A, Holst CR, Latham JC, Bruegger JJ, Ulas G, McCusker KP, Amagata A,
847 Davis D, Hoff KG, Kahn-Kirby AH *et al.* Vitamin E hydroquinone is an endogenous
848 regulator of ferroptosis via redox control of 15-lipoxygenase. *PLOS ONE*
849 2018;**13**:e0201369.

850 Hornick JE, Duncan FE, Shea LD, Woodruff TK. Isolated primate primordial follicles
851 require a rigid physical environment to survive and grow in vitro. *Hum Reprod*
852 2012;**27**:1801-1810.

Hovatta O, Wright C, Krausz T, Hardy K, Winston RML. Human primordial, primary and secondary ovarian follicles in long-term culture: effect of partial isolation. *Hum Reprod* 1999;**14**:2519-2524.

Hu W, Zhang Y, Wang D, Yang T, Qi J, Zhang Y, Jiang H, Zhang J, Sun B, Liang S. Iron Overload-Induced Ferroptosis Impairs Porcine Oocyte Maturation and Subsequent Embryonic Developmental Competence in vitro. *Front Cell Dev Biol* 2021;**9**.

Hulshof SCJ, Figueiredo JR, Beckers JF, Bevers MM, van der Donk JA, van den Hurk R. Effects of fetal bovine serum, FSH and 17β-estradiol on the culture of bovine preantral follicles. *Theriogenology* 1995;**44**:217-226.

Ikeda Y, Satoh A, Horinouchi Y, Hamano H, Watanabe H, Imao M, Imanishi M, Zamami Y, Takechi K, Izawa-Ishizawa Y *et al.* Iron accumulation causes impaired myogenesis correlated with MAPK signaling pathway inhibition by oxidative stress. *FASEB J* 2019;**33**:9551-9564.

Jia Z-C, Li Y-Q, Zhou B-W, Xia Q-C, Wang P-X, Wang X-X, Sun Z-G, Guo Y. Transcriptomic profiling of human granulosa cells between women with advanced maternal age with different ovarian reserve. *J Assist Reprod Genet* 2023;**40**:2427-2437.

Jiang X, Stockwell BR, Conrad M. Ferroptosis: mechanisms, biology and role in disease. *Nat Rev Mol Cell Biol* 2021;**22**:266-282.

Jiang Y, Yu Y, Pan Z, Glandorff C, Sun M. Ferroptosis: a new hunter of hepatocellular carcinoma. *Cell Death Discov* 2024;**10**.

Kanehisa M. KEGG: Kyoto Encyclopedia of Genes and Genomes. *Nucleic Acids Res* 2000;**28**:27-30.

Kanehisa M. Toward understanding the origin and evolution of cellular organisms. *Protein Sci* 2019;**28**:1947-1951.

Kanehisa M, Furumichi M, Sato Y, Kawashima M, Ishiguro-Watanabe M. KEGG for taxonomy-based analysis of pathways and genomes. *Nucleic Acids Res* 2023;**51**:D587-D592.

Katska L, Rynska B. The isolation and in vitro culture of bovine preantral and early antral follicles of different size classes. *Theriogenology* 1998;**50**:213-222.

Kolb JP, Oguin TH, Oberst A, Martinez J. Programmed Cell Death and Inflammation: Winter Is Coming. *Trends Immunol* 2017;**38**:705-718.

Kolde R. Pheatmap: pretty heatmaps. *R package version* 2012;**1**:726.

Koppula P, Zhuang L, Gan B. Cystine transporter SLC7A11/xCT in cancer: ferroptosis, nutrient dependency, and cancer therapy. *Protein Cell* 2021;**12**:599-620.

Krassowski M. ComplexUpset. DOI: 10.5281/zenodo.3700590. 2020.

Langbeen A, Jorssen EP, Fransen E, Rodriguez AP, Garcia MC, Leroy JL, Bols PE. Characterization of freshly retrieved preantral follicles using a low-invasive, mechanical isolation method extended to different ruminant species. *Zygote* 2015;**23**:683-694.

Lex A. UpSet: Visualization of Intersecting Sets. *IEEE Transactions on Visualization and Computer Graphics* 2014;**20**:1983-1992.

Li-Ping Z, Da-Lei Z, Jian H, Liang-Quan X, Ai-Xia X, Xiao-Yu D, Dan-Feng T, Yue-Hui Z. Proto-oncogene c-erbB2 initiates rat primordial follicle growth via PKC and MAPK pathways. *Reprod Biol Endocrinol* 2010;**8**:66.

Li F-J, Long H-Z, Zhou Z-W, Luo H-Y, Xu S-G, Gao L-C. System Xc−/GSH/GPX4 axis: An important antioxidant system for the ferroptosis in drug-resistant solid tumor therapy. *Front Pharmacol* 2022;**13**.

Li L, Chen W, Liang Y, Ma H, Li W, Zhou Z, Li J, Ding Y, Ren J, Lin J *et al.* The Gβγ-Src signaling pathway regulates TNF-induced necroptosis via control of necrosome translocation. *Cell Res* 2014;**24**:417-432.

Liao Y, Wang J, Jaehnig EJ, Shi Z, Zhang B. WebGestalt 2019: gene set analysis toolkit with revamped UIs and APIs. *Nucleic Acids Res* 2019;**47**:W199-W205.

Lima-Verde IB, Matos MHT, Bruno JB, Martins FS, Santos RR, Báo SN, Luque MCA, Vieira GAB, Silveira ER, Rodrigues APR *et al.* Effects of α-tocopherol and ternatin antioxidants on morphology and activation of goat preantral follicles in vitro cultured. *Arq Bras Med Vet Zootec* 2009;**61**:57-65.

Liu Y, Zhou L, Xu Y, Li K, Zhao Y, Qiao H, Xu Q, Zhao J. Heat Shock Proteins and Ferroptosis. *Front Cell Dev Biol* 2022;**10**:864635.

Love MI, Huber W, Anders S. Moderated estimation of fold change and dispersion for RNA-seq data with DESeq2. *Genome Biol* 2014;**15**:550.

Lucia Dos Santos Silva R, de Sousa Barberino R, Tavares de Matos MH. Impact of antioxidant supplementation during in vitro culture of ovarian preantral follicles: A review. *Theriogenology* 2023;**207**:110-122.

Luciano AM, Barros RG, Soares ACS, Buratini J, Lodde V, Franciosi F. Recreating the Follicular Environment: A Customized Approach for In Vitro Culture of Bovine Oocytes Based on the Origin and Differentiation State. *Methods Mol Biol* 2021;**2273**:1-15.

Lung DK, Reese RM, Alarid ET. Intrinsic and Extrinsic Factors Governing the Transcriptional Regulation of ESR1. *Horm Cancer* 2020;**11**:129-147.

Marini F, Binder H. pcaExplorer: an R/Bioconductor package for interacting with RNA-seq principal components. *BMC Bioinformatics* 2019;**20**.

Marino M, Galluzzo P, Ascenzi P. Estrogen Signaling Multiple Pathways to Impact Gene Transcription. *Curr Genomics* 2006;**7**:497-508.

927 McDonnell SP, Candelaria JI, Morton AJ, Denicol AC. Isolation of Small Preantral
928 Follicles from the Bovine Ovary Using a Combination of Fragmentation,
929 Homogenization, and Serial Filtration. *J Vis Exp* 2022:e64423.

930 McGee EA, Hsueh AJ. Initial and cyclic recruitment of ovarian follicles. *Endocr Rev*
931 2000;**21**:200-214.

932 Mclaughlin M, Albertini DF, Wallace WHB, Anderson RA, Telfer EE. Metaphase II
933 oocytes from human unilaminar follicles grown in a multi-step culture system. *Mol Hum*
934 *Reprod* 2018;**24**:135-142.

935 McLaughlin M, Bromfield JJ, Albertini DF, Telfer EE. Activin promotes follicular
936 integrity and oogenesis in cultured pre-antral bovine follicles. *Mol Hum Reprod*
937 2010;**16**:644-653.

938 Méndez M, Fabregues F, Ferreri J, Calafell JM, Villarino A, Otero J, Farre R, Carmona
939 F. Biomechanical characteristics of the ovarian cortex in POI patients and functional
940 outcomes after drug-free IVA. *J Assist Reprod Genet* 2022;**39**:1759-1767.

941 Modina SC, Tessaro I, Lodde V, Franciosi F, Corbani D, Luciano AM. Reductions in
942 the number of mid-sized antral follicles are associated with markers of premature
943 ovarian senescence in dairy cows. *Reprod Fertil Dev* 2014;**26**:235-244.

944 Monferini N, Dey P, Donadini L, Katsakoglou N, Franciosi F, Lodde V, Luciano AM.
945 Age-dependent high-yield isolation of primordial, primary, and early secondary follicles
946 from the bovine ovarian cortex. *Reproduction* 2024;**167**:e240060.

947 Montojo J, Zuberi K, Rodriguez H, Kazi F, Wright G, Donaldson SL, Morris Q, Bader
948 GD. GeneMANIA Cytoscape plugin: fast gene function predictions on the desktop.
949 *Bioinformatics* 2010;**26**:2927-2928.

950 Mostafavi S, Ray D, Warde-Farley D, Grouios C, Morris Q. GeneMANIA: a real-time
951 multiple association network integration algorithm for predicting gene function.
952 *Genome Biol* 2008;**9**:S4.

953 Moussay E, Kaoma T, Baginska J, Muller A, Van Moer K, Nicot N, Nazarov PV, Vallar
954 L, Chouaib S, Berchem G *et al.* The acquisition of resistance to TNFα in breast cancer
955 cells is associated with constitutive activation of autophagy as revealed by a
956 transcriptome analysis using a custom microarray. *Autophagy* 2011;**7**:760-770.

957 Nagamatsu G, Shimamoto S, Hamazaki N, Nishimura Y, Hayashi K. Mechanical
958 stress accompanied with nuclear rotation is involved in the dormant state of mouse
959 oocytes. *Sci Adv* 2019;**5**:eaav9960.

960 Nilsson E, Dole G, Skinner MK. Neurotrophin NT3 promotes ovarian primordial to
961 primary follicle transition. *Reproduction* 2009;**138**:697-707.

962 O'Brien MJ, Pendola JK, Eppig JJ. A Revised Protocol for In Vitro Development of
963 Mouse Oocytes from Primordial Follicles Dramatically Improves Their Developmental
964 Competence1. *Biol Reprod* 2003;**68**:1682-1686.

965 Oeckinghaus A, Hayden MS, Ghosh S. Crosstalk in NF-κB signaling pathways. *Nat*
966 *Immunol* 2011;**12**:695-708.

967 Otasek D, Morris JH, Bouças J, Pico AR, Demchak B. Cytoscape Automation:
968 empowering workflow-based network analysis. *Genome Biol* 2019;**20**:185.

969 Pargianas M, Kosmas I, Papageorgiou K, Kitsou C, Papoudou-Bai A, Batistatou A,
970 Markoula S, Salta S, Dalkalitsis A, Kolibianakis S *et al.* Follicle inhibition at the
971 primordial stage without increasing apoptosis, with a combination of everolimus,
972 verapamil. *Mol Biol Rep* 2020;**47**:8711-8726.

973 Passos MJ, Vasconcelos GL, Silva AWB, Brito IR, Saraiva MVA, Magalhães DM,
974 Costa JJN, Donato MAM, Ribeiro RP, Cunha EV *et al.* Accelerated growth of bovine
975 preantral follicles in vitro after stimulation with both FSH and BMP-15 is accompanied
976 by ultrastructural changes and increased atresia. *Theriogenology* 2013;**79**:1269-1277.

977 Patro R, Duggal G, Love MI, Irizarry RA, Kingsford C. Salmon provides fast and bias-
978 aware quantification of transcript expression. *Nat Methods* 2017;**14**:417-419.

979 Patton BK, Madadi S, Pangas SA. Control of ovarian follicle development by TGF-β
980 family signaling. *Curr Opin Endocr Metab Res* 2021;**18**:102-110.

981 Paulino L, Barroso PAA, Silva AWB, Souza ALP, Bezerra FTG, Silva BR, Donato
982 MMA, Peixoto CA, Silva JRV. Effects of epidermal growth factor and progesterone on
983 development, ultrastructure and gene expression of bovine secondary follicles
984 cultured in vitro. *Theriogenology* 2020;**142**:284-290.

985 Paulino L, Cunha EV, Barbalho Silva AW, Souza GB, Lopes EPF, Donato MAM,
986 Peixoto CA, Matos-Brito BG, van den Hurk R, Silva JRV. Effects of tumour necrosis
987 factor-alpha and interleukin-1 beta on in vitro development of bovine secondary
988 follicles. *Reprod Domest Anim* 2018;**53**:997-1005.

989 Saha S, Shimizu M, Geshi M, Izaike Y. In vitro culture of bovine preantral follicles.
990 *Anim Reprod Sci* 2000;**63**:27-39.

991 Salama M, Isachenko V, Isachenko E, Rahimi G, Mallmann P. Updates in preserving
992 reproductive potential of prepubertal girls with cancer: Systematic review. *Crit Rev*
993 *Oncol Hematol* 2016;**103**:10-21.

994 Samson AL, Garnish SE, Hildebrand JM, Murphy JM. Location, location, location: A
995 compartmentalized view of TNF-induced necroptotic signaling. *Sci Signal*
996 2021;**14**:eabc6178.

997 Silva JRV, Lima FEO, Souza ALP, Silva AWB. Interleukin-1β and TNF-α systems in
998 ovarian follicles and their roles during follicular development, oocyte maturation and
999 ovulation. *Zygote* 2020;**28**:270-277.

1000 Simon LE, Kumar TR, Duncan FE. In vitro ovarian follicle growth: a comprehensive
1001 analysis of key protocol variables. *Biol Reprod* 2020;**103**:455-470.

1002 Sun J, Li X. Growth and antrum formation of bovine primary follicles in long-term
1003 culture in vitro. *Reprod Biol* 2013;**13**:221-228.

1004 Sun X, Klinger FG, Liu J, De Felici M, Shen W, Sun X. miR-378-3p maintains the size
1005 of mouse primordial follicle pool by regulating cell autophagy and apoptosis. *Cell*
1006 *Death Dis* 2020;**11**:737.

1007 Tan W, Dai F, Yang D, Deng Z, Gu R, Zhao X, Cheng Y. MiR-93-5p promotes
1008 granulosa cell apoptosis and ferroptosis by the NF-kB signaling pathway in polycystic
1009 ovary syndrome. *Front Immunol* 2022;**13**:967151.

1010 Tanzer MC. A proteomic perspective on TNF-mediated signalling and cell death.
1011 *Biochem Soc Trans* 2022;**50**:13-20.

1012 Telfer EE, Grosbois J, Odey YL, Rosario R, Anderson RA. Making a good egg: human
1013 oocyte health, aging, and in vitro development. *Physiol Rev* 2023;**103**:2623-2677.

1014 Telfer EE, Sakaguchi K, Clarkson YL, McLaughlin M. In vitro growth of immature
1015 bovine follicles and oocytes. *Reprod Fertil Dev* 2019;**32**:1-6.

1016 Van Loo G, Bertrand MJM. Death by TNF: a road to inflammation. *Nat Rev Immunol*
1017 2023;**23**:289-303.

1018 Vilela JMV, Dolmans MM, Amorim CA. Ovarian tissue transportation: a systematic
1019 review. *Reprod Biomed Online* 2021;**42**:351-365.

1020 Wang S, Zheng Y, Li J, Yu Y, Zhang W, Song M, Liu Z, Min Z, Hu H, Jing Y *et al.*
1021 Single-Cell Transcriptomic Atlas of Primate Ovarian Aging. *Cell* 2020a;**180**:585-
1022 600.e519.

1023 Wang X, Tan X, Zhang J, Wu J, Shi H. The emerging roles of MAPK-AMPK in
1024 ferroptosis regulatory network. *Cell Commun Signal* 2023;**21**:200.

1025 Wang Y, Zhang H, Chen Q, Jiao F, Shi C, Pei M, Lv J, Zhang H, Wang L, Gong Z.
1026 TNF-alpha/HMGB1 inflammation signalling pathway regulates pyroptosis during liver
1027 failure and acute kidney injury. *Cell Prolif* 2020b;**53**:e12829.

1028 Wang Z-P, Mu X-Y, Guo M, Wang Y-J, Teng Z, Mao G-P, Niu W-B, Feng L-Z, Zhao
1029 L-H, Xia G-L. Transforming Growth Factor-β Signaling Participates in the Maintenance
1030 of the Primordial Follicle Pool in the Mouse Ovary. *J Biol Chem* 2014;**289**:8299-8311.

1031 Warde-Farley D, Donaldson SL, Comes O, Zuberi K, Badrawi R, Chao P, Franz M,
1032 Grouios C, Kazi F, Lopes CT *et al.* The GeneMANIA prediction server: biological
1033 network integration for gene prioritization and predicting gene function. *Nucleic Acids*
1034 *Res* 2010;**38**:W214-W220.

1035 Wright CJ, Cari EL, Sandoval J, Bales E, Sam PK, Zarate MA, Polotsky AJ, Kallen
1036 AN, Johnson J. Control of Murine Primordial Follicle Growth Activation by IκB/NFκB
1037 Signaling. *Reprod Sci* 2020;**27**:2063-2074.

1038 Wu J, Feng Z, Chen L, Li Y, Bian H, Geng J, Zheng Z-H, Fu X, Pei Z, Qin Y *et al.* TNF
1039 antagonist sensitizes synovial fibroblasts to ferroptotic cell death in collagen-induced
1040 arthritis mouse models. *Nat Commun* 2022;**13**:676.

1041 Xu X, Li Y, Wu Y, Wang M, Lu Y, Fang Z, Wang H, Li Y. Increased ATF2 expression
1042 predicts poor prognosis and inhibits sorafenib-induced ferroptosis in gastric cancer.
1043 *Redox Biol* 2023;**59**:102564.

1044 Zeng W, Wang F, Cui Z, Zhang Y, Li Y, Li N, Mao Z, Zhang H, Liu Y, Miao Y *et al.*
1045 Inhibition of ferroptosis counteracts the advanced maternal age-induced oocyte
1046 deterioration. *Cell Death Differ* 2025.

1047 Zhang J, Su T, Fan Y, Cheng C, Xu L, LiTian. Spotlight on iron overload and
1048 ferroptosis: Research progress in female infertility. *Life Sci* 2024;**340**:122370.

1049 Zhang T, He M, Zhang J, Tong Y, Chen T, Wang C, Pan W, Xiao Z. Mechanisms of
1050 primordial follicle activation and new pregnancy opportunity for premature ovarian
1051 failure patients. *Front Physiol* 2023;**14**:1113684.

1052 Zhang Y, Yan Z, Qin Q, Nisenblat V, Chang HM, Yu Y, Wang T, Lu C, Yang M, Yang
1053 S *et al.* Transcriptome Landscape of Human Folliculogenesis Reveals Oocyte and
1054 Granulosa Cell Interactions. *Mol Cell* 2018;**72**:1021-1034 e1024.

1055 Zhao Y, Zhang Y, Li J, Zheng N, Xu X, Yang J, Xia G, Zhang M. MAPK3/1 participates
1056 in the activation of primordial follicles through mTORC1-KITL signaling. *J Cell Physiol*
1057 2018;**233**:226-237.

1058 Zhou J, Lin L, Liu L, Wang J, Xia G, Wang C. The transcriptome reveals the molecular
1059 regulatory network of primordial follicle depletion in obese mice. *Fertil Steril*
1060 2023a;**120**:899-910.

1061 Zhou N, Yuan X, Du Q, Zhang Z, Shi X, Bao J, Ning Y, Peng L. FerrDb V2: update of
1062 the manually curated database of ferroptosis regulators and ferroptosis-disease
1063 associations. *Nucleic Acids Res* 2023b;**51**:D571-D582.

1064 Zoheir KM, Harisa GI, Allam AA, Yang L, Li X, Liang A, Abd-Rabou AA, Harrath AH.
1065 Effect of alpha lipoic acid on in vitro development of bovine secondary preantral
1066 follicles. *Theriogenology* 2017;**88**:124-130.

1067

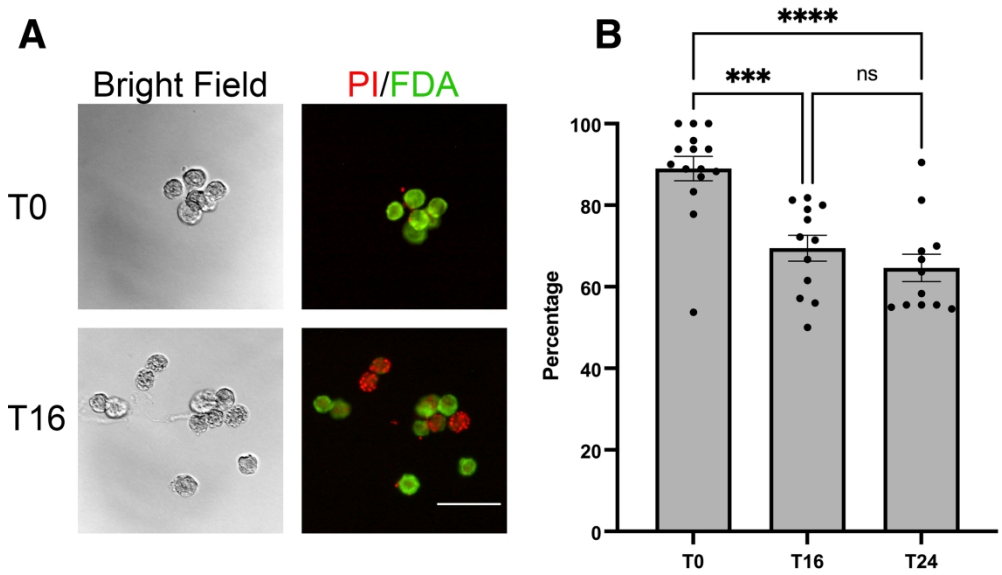

Figure 1. (A) Viability assessment of PMF T0 (freshly collected primordial follicles, control) and PMF T16 (primordial follicles cultured for 16 h) using PI and FDA. Scale bar = 100 µm. (B) Viability of PMF after 0, 16, and 24 h of culture, T0 (N= 311), T16 (N=175), and T24 (N=199), respectively. The experiment was repeated 5 times (n=5). **** indicate significant differences between groups where p ≤0.0001, *** indicate significant differences between groups where p<0.005; ns: not significant.

161x93mm (600 x 600 DPI)

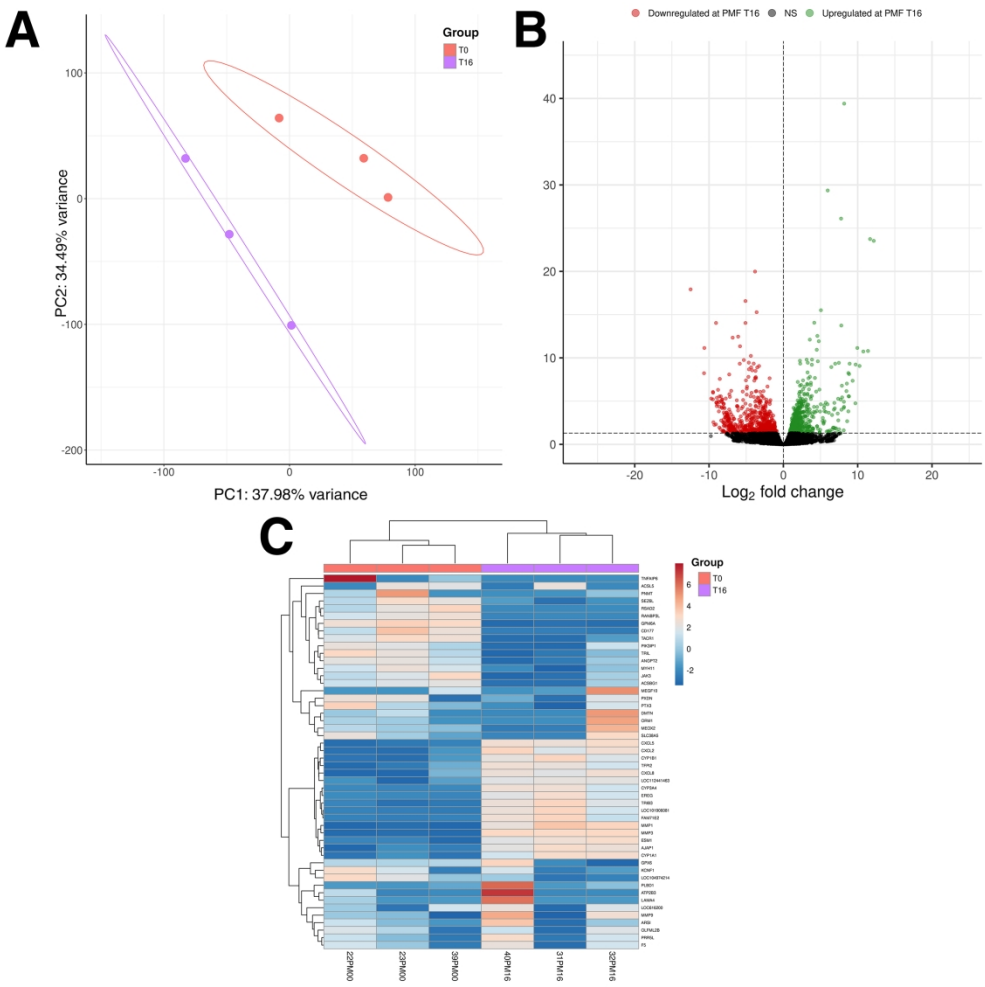

Figure 2. (A) Principal Component Analysis (PCA) plot shows apparent clustering of PMF T0 (freshly collected primordial follicles, control) and T16 (primordial follicles cultured for 16 h). (B) Volcano plot of differential gene expression (DGE) analysis shows up and downregulated differentially expressed genes (DEGs) (FDR<0.1) determined between PMF T0 and PMF T16 represented by green and red dots, respectively. (C) Heatmap of top 50 most variable genes. The heatmap shows normalized gene expression by regularized log transformation.

168x165mm (600 x 600 DPI)

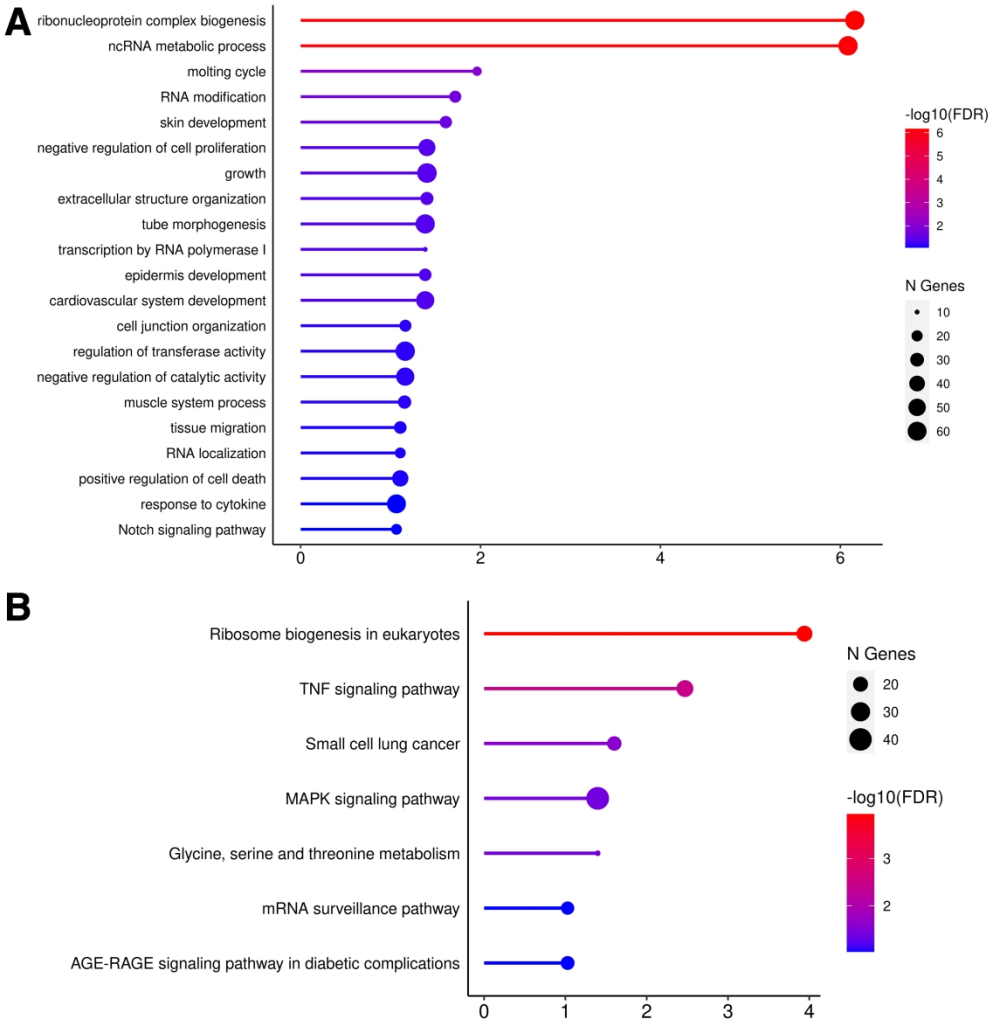

Figure 3. Over Representation Analysis of 1949 differentially expressed genes (DEGs) shows enriched (A) GO: Biological Processes. (B) KEGG pathways. The ontological terms were enriched at FDR < 0.1. DEGs (FDR < 0.1) were determined between PMF T0 (freshly collected primordial follicles, control) and PMF T16 (primordial follicles cultured for 16 h).

170x176mm (600 x 600 DPI)

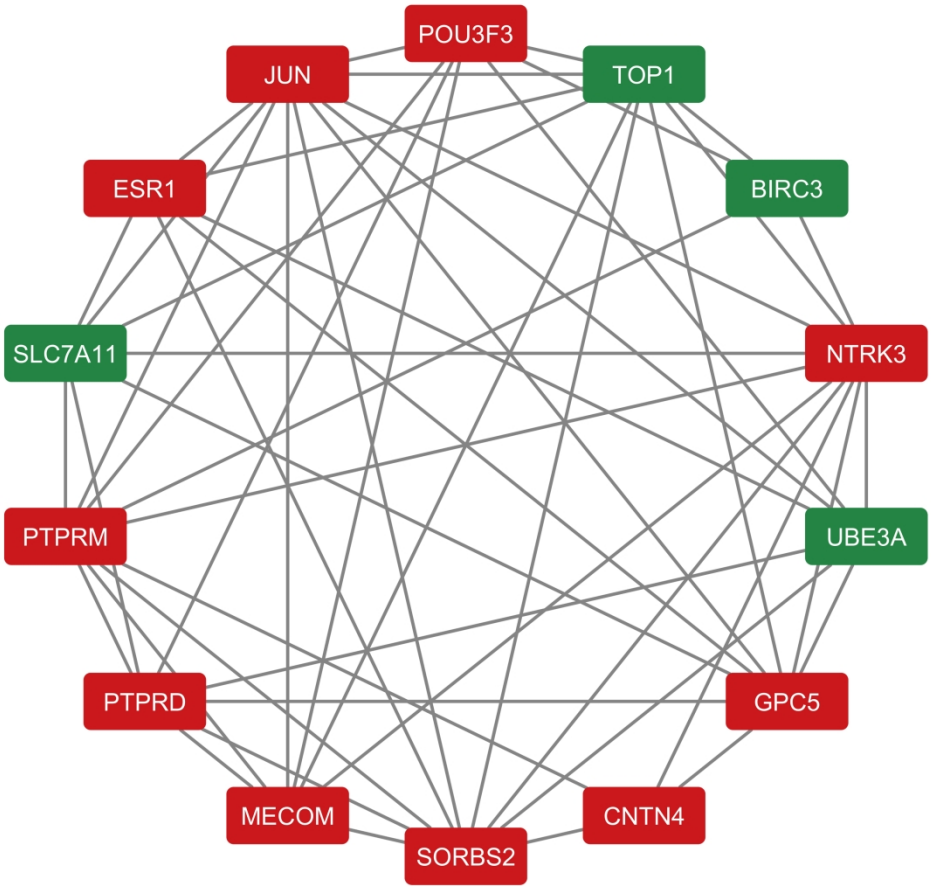

Figure 4. Hub gene identification analysis performed with CytoHubba identified the top 14 hub genes. Node representations: Green and red rectangles represent up and downregulated differentially expressed genes (DEGs), respectively, determined between PMF T0 (freshly collected primordial follicles, control) and PMF T16 (primordial follicles cultured for 16 h) (FDR < 0.1)

133x127mm (600 x 600 DPI)

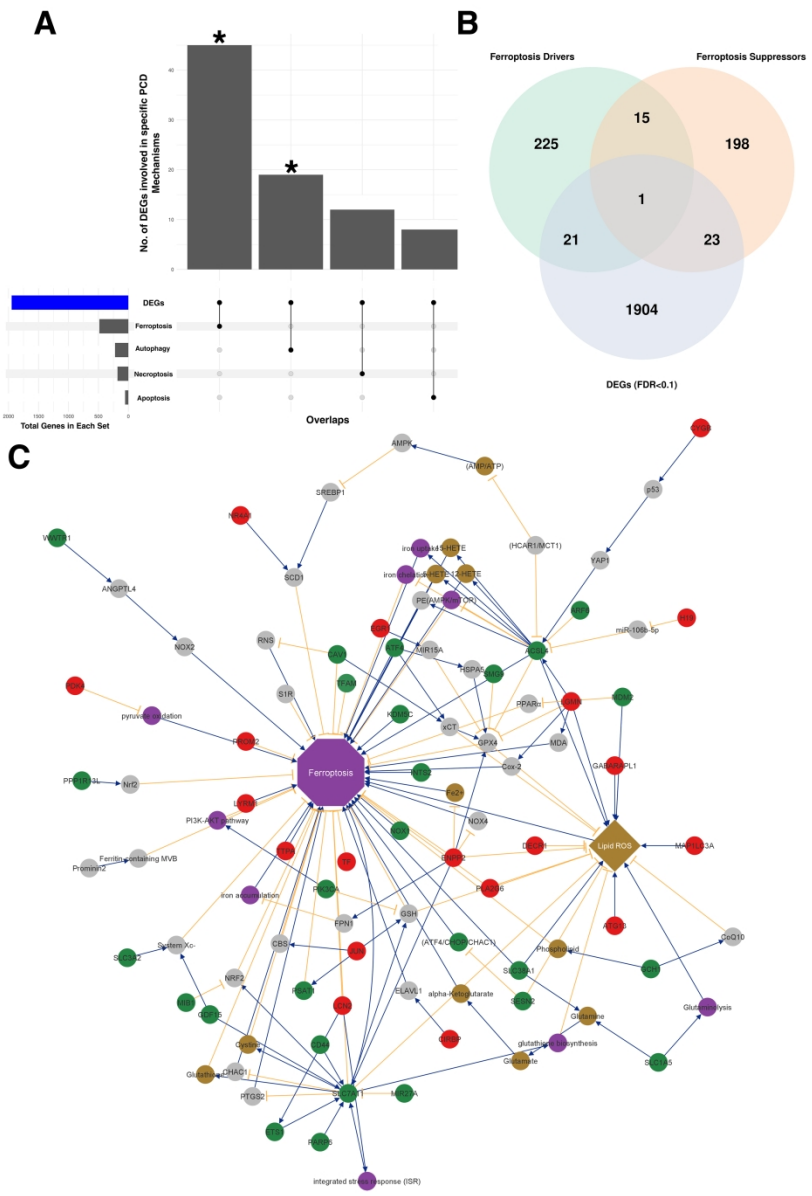

Figure 5. (A) UpSet plot of differentially expressed genes (DEGs) determined between PMF T0 (freshly collected primordial follicles, control) and PMF T16 (primordial follicles cultured for 16 h) (FDR < 0.1) overlapped with genes involved in ferroptosis, autophagy, necroptosis, and apoptosis. (*represents programmed cell death (PCD) mechanisms significantly associated with the DEGs (B) Venn diagram of ferroptosis drivers and suppressors differentially expressed between PMF T16 and T0. (C) Node representations: Green and red circles represent up and downregulated DEGs, respectively; grey circles represent genes not significantly differentially expressed in our dataset, and purple circles represent pathways or processes. Edge representations: Yellow lines represent inhibition, and blue lines represent activation of a gene, molecule, or pathway.

165x239mm (600 x 600 DPI)

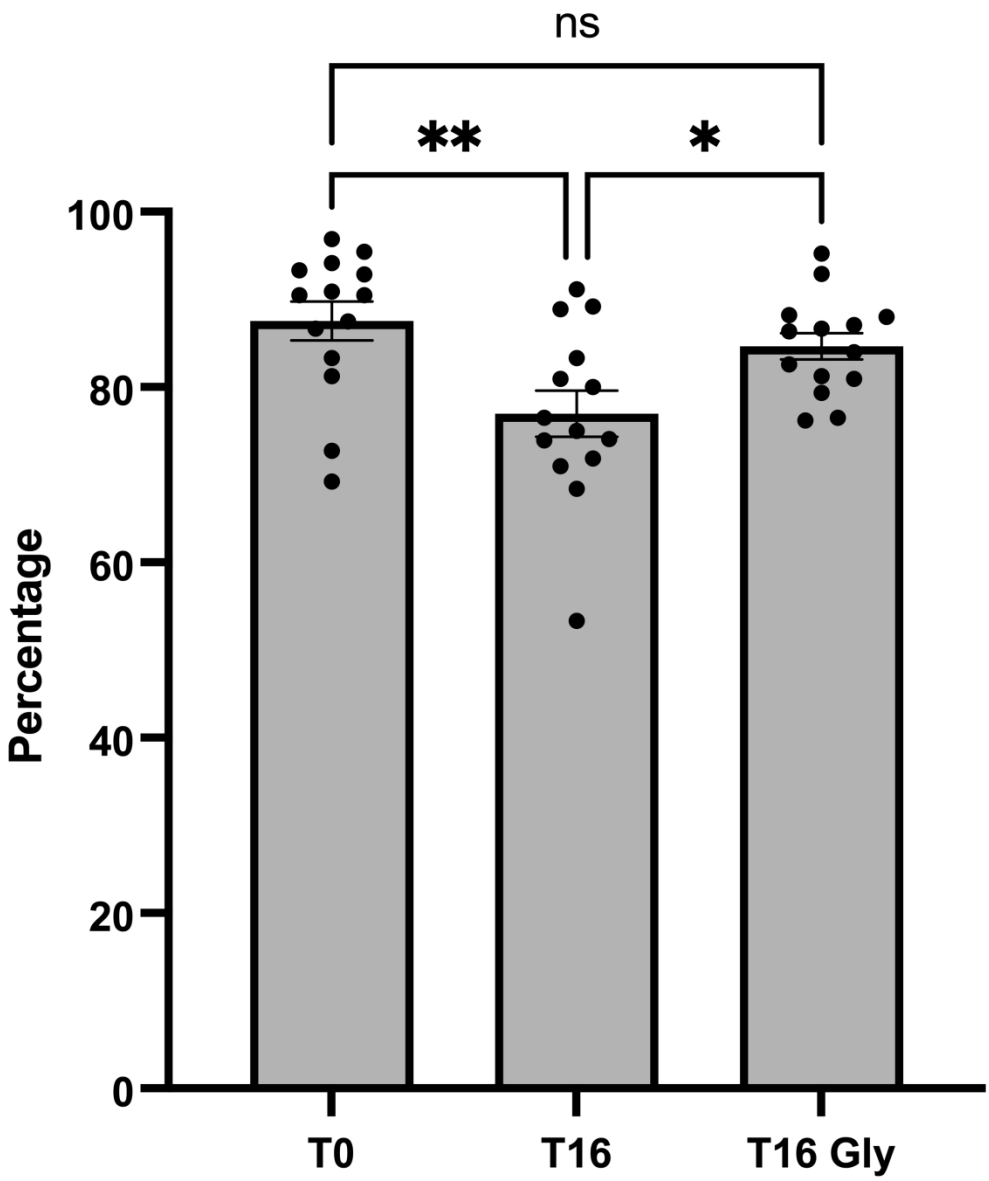

Figure 6. The graph shows the viability of PMF (primordial follicles) after 0 h and 16 h of culture with 6 mM glycine, T0 (N=334), T16 (N=349), and T24 (N=368), respectively. The experiment was repeated 5 times (n=5). ** indicates significant differences between groups where $p \leq 0.005$, * indicates significant differences between groups where $p \leq 0.05$ and ns: not significant.

114x138mm (600 x 600 DPI)

Table 1. Number of primordial follicles retrieved after at T0 or T16 for RNA sequencing in each replicate.

Samples	PMF T0 (N)	PMF T16 (N)
Replicate 1	119	209
Replicate 2	202	133
Replicate 3	210	165

PM, primordial follicle; T0, start of culture; T16, after 16h in culture